

(MGS)²: Unifying Micro-Geometric Scale and Macro-Geometric Structure for Cross-View Geo-Localization

Minglei Li[†], Mengfan He[†], Chao Chen and Ziyang Meng

Abstract— Cross-view geo-localization (CVGL) is pivotal for GNSS-denied UAV navigation but remains brittle under the drastic geometric misalignment between oblique aerial views and orthographic satellite references. Existing methods predominantly operate within a 2D manifold, neglecting the underlying 3D geometry where view-dependent vertical facades (macro-structure) and scale variations (micro-scale) severely corrupt feature alignment. To bridge this gap, we propose (MGS)², a geometry-grounded framework. The core of our innovation is the Macro-Geometric Structure Filtering (MGSF) module. Unlike pixel-wise matching sensitive to noise, MGSF leverages dilated geometric gradients to physically filter out high-frequency facade artifacts while enhancing the view-invariant horizontal plane, directly addressing the domain shift. To guarantee robust input for this structural filtering, we explicitly incorporate a Micro-Geometric Scale Adaptation (MGSA) module. MGSA utilizes depth priors to dynamically rectify scale discrepancies via multi-branch feature fusion. Furthermore, a Geometric-Appearance Contrastive Distillation (GACD) loss is designed to strictly discriminate against oblique occlusions. Extensive experiments demonstrate that (MGS)² achieves state-of-the-art performance, recording a Recall@1 of 97.5% on University-1652 and 97.02% on SUES-200. Furthermore, the framework exhibits superior cross-dataset generalization against geometric ambiguity. The code is available at: <https://github.com/GabrielLi1473/MGS-Net>.

I. INTRODUCTION

Unmanned Aerial Vehicles (UAVs) are revolutionizing applications from urban monitoring to logistics [1], [2], yet their autonomy relies on robust localization. Since Global Navigation Satellite Systems (GNSS) are often rendered unreliable by signal jamming and multipath effects in complex urban environments [3], Visual Cross-View Geo-Localization (CVGL), matching real-time onboard views against satellite orthophotos, has emerged as a critical navigation alternative [4] [5].

CVGL is challenged by extreme domain shifts: UAV views contain rich multi-perspective imagery, while satellite views are strictly orthographic [6]. To bridge this gap, early CNN-based metric learning [7], [8] has evolved into Vision Transformer (ViT) approaches like TransGeo [9] and L2LTR [10], which leverage global context and polar transformations. Recent works have further refined feature granularity through contrastive attribute mining [11], orthogonal fusion [12], or ground structure modeling [13].

This work was supported by ... († indicates equal contribution) (Corresponding author: Ziyang Meng)

The authors are with Department of Precision Instrument, Tsinghua University, Beijing 100084, China (email: liminglei25@mails.tsinghua.edu.cn, hmf21@mails.tsinghua.edu.cn, cc15538965027@163.com, ziyangmeng@mail.tsinghua.edu.cn).

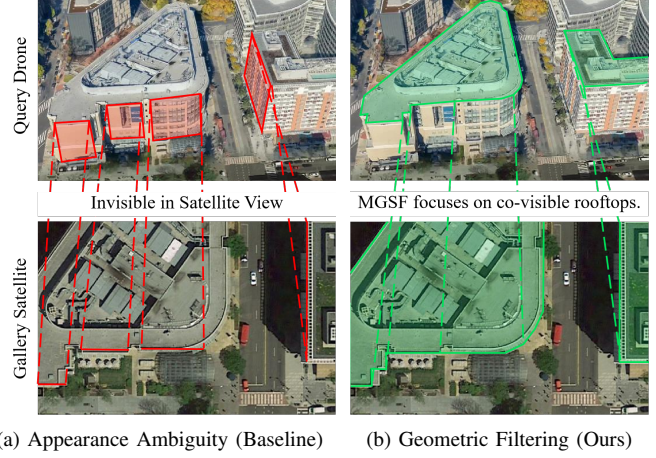


Fig. 1. From Texture Dependency to Geometric Grounding. (a) Visual Ambiguity: Existing methods often overfit to view-dependent vertical facades (red boxes) that are invisible in the satellite orthophoto, leading to retrieval failure. (b) Our Solution: By explicitly modeling 3D macro-geometric structures, our MGS-Net filters out these vertical artifacts via MGSF and robustly focuses on view-invariant rooftops (green boxes), ensuring consistent cross-view alignment. The image materials are from the University-1652 dataset.

Despite these advancements, existing methods lack explicit 3D structural awareness. In dense urban scenarios, the primary bottleneck is macro-level structural noise: oblique UAV images feature a greater number of vertical facades that serve as high-frequency noise invisible in satellite references. This structural gap is further complicated by micro-level scale ambiguity, where texture sizes vary drastically with depth, preventing effective feature alignment. Merely concatenating depth maps is insufficient, as raw monocular estimation lacks the semantic capacity to distinguish valid matching surfaces (horizontal plane) from invalid ones (facade).

We propose (MGS)² to shift from passive texture matching to active geometric filtering. Our central insight is that robust alignment hinges on explicitly filtering out view-dependent vertical structures. To this end, we introduce the Macro-Geometric Structure Filtering (MGSF) module as the backbone of our framework. MGSF computes dilated geometric gradients to capture large-scale planar trends, effectively suppressing vertical facade features while preserving horizontal plane structures.

Complementing this core mechanism, we introduce the Micro-Geometric Scale Adaptation (MGSA) module to resolve the scale ambiguity that often undermines structural analysis. By applying depth priors and regressing dynamic attention weights, MGSA fuses features from three different scale-expanding branches. Finally, the Geometric-Appearance Contrastive Distillation (GACD) Loss discrim-

inates against oblique occlusions by enforcing a margin between horizontal plane and facade activations.

Our contributions can be summarized as follows:

- We pioneer a geometry-grounded CVGL paradigm via (MGS)². To the best of our knowledge, this is the first framework to explicitly leverage 3D structural constraints to bridge the oblique-orthogonal gap, shifting from 2D texture matching to 3D geometric alignment.
- We propose a synergistic Micro-Macro Geometric Alignment mechanism. This integrates the Macro-Geometric Structure Filtering (MGSF) module to physically filter view-dependent vertical artifacts, supported by the Micro-Geometric Scale Adaptation (MGSA) module, which utilizes depth priors to rectify scale ambiguity.
- We introduce the Geometric-Appearance Contrastive Distillation (GACD) Loss. This ranking-based objective explicitly mines vertical facades as hard negatives, compelling the network to discriminate against oblique occlusions.
- We achieve new state-of-the-art performance. Our method achieves record-breaking Recall@1 scores of 97.5% on University-1652 and 97.0% on SUES-200, accompanied by strong cross-dataset generalization capabilities.

The remainder of this paper is organized as follows: Section II reviews related work in CVGL and multi-modal fusion. Section III details the architecture of (MGS)². Section IV presents comprehensive experiments and ablation studies. Finally, Section V concludes the paper.

II. RELATED WORK

A. Foundation Models and Cross-View Geo-Localization

Cross-view geo-localization (CVGL) is fundamentally formulated as a metric learning problem, aiming to embed location-dependent visual cues into a shared latent space [14]. Early pioneering works predominantly relied on Convolutional Neural Networks (CNNs). Approaches like CVM-Net [15] utilized NetVLAD for global descriptor aggregation, while RK-Net [16] incorporated keypoint detection to focus on discriminative regions.

Recently, the introduction of Vision Transformers (ViT) and large-scale Foundation Models has marked a paradigm shift. TransGeo [9] leveraged self-attention with polar transformations to roughly align geometric layouts, while Sample4Geo [17] achieved significant gains via hard-negative mining. Concurrently, foundation models like DINO [18] and DINOv2 [19] have demonstrated exceptional generalization capabilities. Recent works [20], [21] have successfully adapted these pre-trained frozen backbones to UAV localization, utilizing their robust semantic descriptors to mitigate domain shifts. However, despite the powerful representation capabilities of these RGB-based foundation models, they inherently operate within a 2D manifold. They treat the scene as a planar surface, neglecting the micro-level scale ambiguity caused by depth variations, often overfitting to transient

artifacts (e.g., dynamic vehicles) rather than geometrically consistent structures.

B. Fine-Grained Alignment and Semantic Fusion

To address the spatial misalignment inherent in global descriptors, research has shifted towards fine-grained semantic alignment [22]. Several approaches integrate high-level semantics to enhance discriminability, utilizing graph convolutional networks [23], semantic concept perception [24], or saliency-aware networks [25] to model layout consistencies. To handle diverse scene characteristics, multi-environment adaptive frameworks like MESAN [26] have been proposed. Other advancements focus on refining feature correspondence through hierarchical distillation [27], ensuring multi-level consistency [28], [29], or unifying retrieval and reranking pipelines [30]. While these methods employ sophisticated semantic mining to align features, they lack a physical mechanism to explicitly reject macro-level structural noise. For instance, a vertical facade often shares similar texture statistics with horizontal roads. Without explicit 3D structural constraints, attention mechanisms often misalign these distinct geometric planes, leading to performance degradation in dense urban environments where vertical structures dominate the UAV view.

C. Geometry-Aware Cross-View Geo-Localization

Recognizing the limitations of pure visual matching, a growing number of studies have begun to incorporate geometric cues. Generative methods like CDM-Net [31] employ diffusion models for view synthesis to bridge the perspective gap, while Wang et al. [32] utilize Neural ODEs for continuous manifold modeling. In broader place recognition tasks, LiDAR-camera fusion [33], [34] has been used to impose metric constraints. However, in standard CVGL where only monocular images are available, most geometry-aware methods simply concatenate estimated depth as an additional input channel [35], [36]. This Input Concatenation strategy is suboptimal as raw monocular depth is often plagued by pixel-level noise and does not explicitly inform the network of structural semantics.

Diverging from implicit fusion or simple concatenation, we propose a geometry-grounded paradigm via (MGS)². We leverage the state-of-the-art Depth Anything 3 [37] to extract explicit depth priors, but distinctively, we decompose alignment into two synergistic processes: Macro-Geometric Structure Filtering (MGSF) to physically filter out vertical artifacts via geometric gradient analysis, and Micro-Geometric Scale Adaptation (MGSA) to rectify depth-induced scale variations. Furthermore, we introduce the GACD Loss to enforce a ranking where view-invariant roof structures are explicitly prioritized over oblique occlusions.

III. METHODOLOGY

A. Overview

Given a query UAV image I_u and a gallery of satellite reference images $\mathcal{S} = \{I_s^i\}_{i=1}^N$, the goal of cross-view geo-localization is to learn a mapping function $\mathcal{F}(\cdot)$ that projects

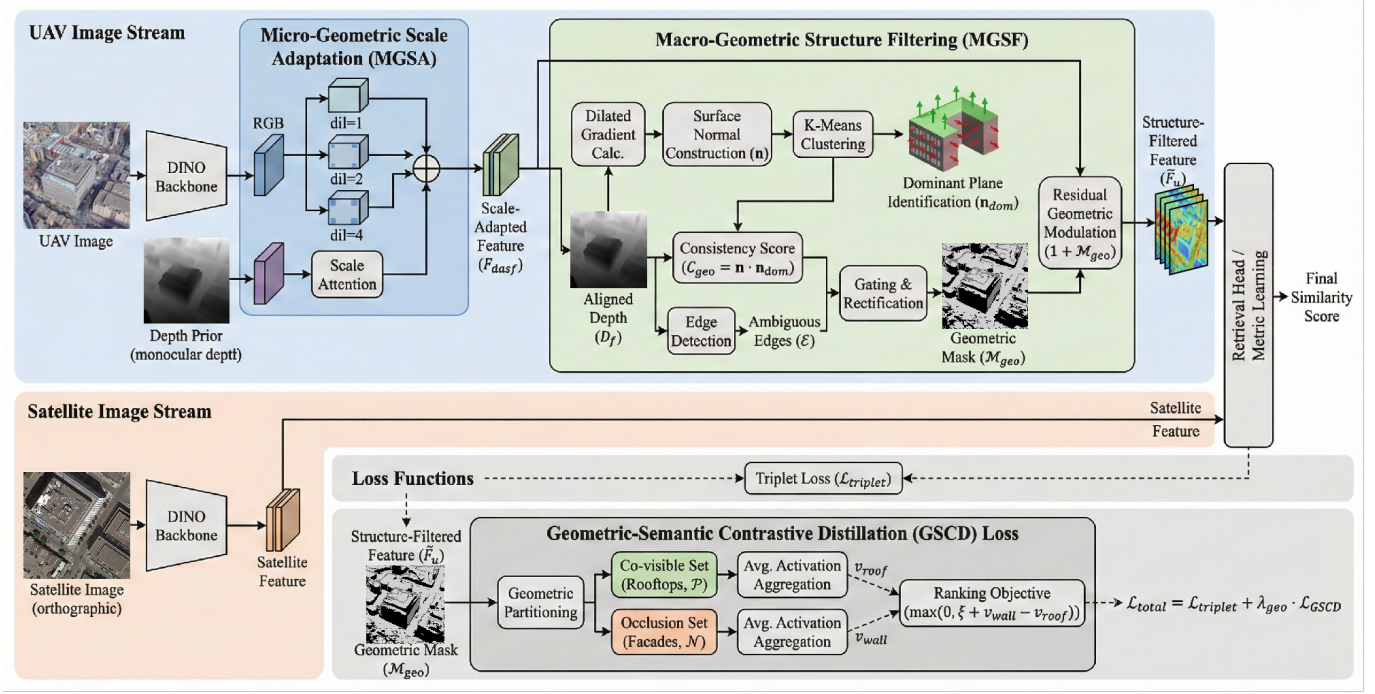


Fig. 2. The overall framework of the proposed (MGS)². It mainly consists of the Micro-Geometric Scale Adaptation (MGSA) module to handle scale variations and the Macro-Geometric Structure Filtering (MGSF) module to suppress view-dependent artifacts.

images from both domains into a shared latent space, where the similarity between matched pairs is maximized. However, the domain gap poses a fundamental challenge: UAV images capture oblique views rich in vertical facades (e.g., walls, windows), whereas satellite images provide orthographic views dominated by horizontal planes (e.g., rooftops, roads). These vertical structures in UAV images act as geometric noise, introducing view-dependent artifacts that degrade retrieval performance. To address this, we propose a geometry-aware framework comprising three novel components in Figure 2:

- Micro-Geometric Scale Adaptation (MGSA): A depth-guided module that dynamically fuses multi-scale features to adapt to varying UAV altitudes.
- Macro-Geometric Structure Filtering (MGSF): A module that leverages coarse depth estimation to suppress vertical artifacts and enhance horizontal surfaces.
- Geometric-Semantic Contrastive Distillation (GACD) Loss: A ranking-based objective that explicitly compels the network to prioritize geometric consistency in the feature space.

B. Micro-Geometric Scale Adaptation (MGSA)

Before addressing macro-structural artifacts, it is critical to mitigate the scale ambiguity caused by varying UAV flight altitudes. We propose a Micro-Geometric Scale Adaptation (MGSA) module that incorporates a Depth-Aware Scale Fusion (DASF) strategy. This module dynamically calibrates the receptive field of RGB features guided by depth cues, ensuring that features are robust to scale variations.

1) *Depth-Aware Scale Fusion (DASF)*: Let $\mathbf{F}_r \in \mathbb{R}^{C \times H \times W}$ denote the initial RGB feature map extracted from the backbone. To capture visual cues at different ranges, DASF generates three parallel scale branches using dilated convolutions with varying dilation rates:

$$\mathbf{F}_{near} = \mathbf{F}_r, \mathbf{F}_{mid} = \phi_{dil=2}(\mathbf{F}_r), \mathbf{F}_{far} = \phi_{dil=4}(\mathbf{F}_r), \quad (1)$$

where $\phi_{dil=k}$ denotes a convolution operation with dilation rate k . These branches are then stacked to form a multi-scale tensor $\mathbf{F}_{stack} \in \mathbb{R}^{B \times 3 \times C \times H \times W}$. To determine the optimal scale contribution for each spatial location, we utilize depth embeddings \mathbf{F}_d as a geometric prior. A prediction head ψ maps these depth features to a spatial weight map, which is normalized via a Softmax function across the scale dimension:

$$\mathbf{W} = \text{Softmax}(\psi(\mathbf{F}_d)), \quad (2)$$

where $\mathbf{W} \in \mathbb{R}^{B \times 3 \times 1 \times H \times W}$ represents the pixel-wise attention weights for the near, mid, and far scales. Finally, the scale-adaptive feature \mathbf{F}_{dasf} is obtained via a weighted fusion followed by a residual connection to preserve original semantic information:

$$\mathbf{F}_{dasf} = \mathbf{F}_r + \sum s \in \{near, mid, far\} \mathbf{W}_s \odot \mathbf{F}_s, \quad (3)$$

The resulting feature map $\mathbf{F}_{dasf} \in \mathbb{R}^{B \times C \times H \times W}$ possesses enhanced scale invariance and serves as the refined input for the subsequent structure filtering module.

C. Macro-Geometric Structure Filtering (MGSF)

We argue that for geo-localization, absolute depth accuracy is secondary to macro-surface orientation. Therefore,

MGSF is designed to extract the Dominant Geometric Normal—a robust statistical prior indicating the likelihood of a surface being a co-visible horizontal plane rather than a vertical occlusion.

1) *Depth-to-Feature Alignment*: Let $F_u = \mathbf{F}_{dasf}$ denote the scale-adapted semantic feature map. We first estimate a monocular depth map D_{raw} and align it with the feature space via adaptive average pooling. This operation acts as a low-pass filter, smoothing out local texture variations while preserving dominant structural trends:

$$D_f = \text{AvgPool}(D_{raw}, (H, W)), \quad (4)$$

where $D_f \in \mathbb{R}^{1 \times H \times W}$ represents the feature-aligned macro-depth.

2) *Macro Gradient via Dilated Convolution*: To capture the orientation of large-scale planar structures while ignoring minor surface roughness, we compute the depth gradients using dilated convolutions. A dilated Sobel operator extends the receptive field:

$$G_x = D_f * S_x^{(r)}, \quad G_y = D_f * S_y^{(r)}, \quad (5)$$

where $*$ denotes convolution with dilation rate r , and (G_x, G_y) represent the macro-geometric gradients.

3) *Dominant Plane Perception via Normal Clustering*: Instead of assuming a rigid vertical axis, we employ a clustering-based strategy to robustly identify co-visible horizontal planes. First, pixel-wise surface normal vectors $\mathbf{n} \in \mathbb{R}^3$ are constructed from the gradients: $\mathbf{n} = \text{Normalize}([-G_x, -G_y, 1])$. To mitigate the impact of depth discontinuities (e.g., building boundaries) which often contain estimation errors, we filter out high-frequency regions based on gradient magnitude. Pixels with $\|\nabla D\| > \tau_{grad}$ are labeled as *ambiguous edges* \mathcal{E} , while the remaining constitute the *flat candidate set* \mathcal{S}_{flat} . We then perform K-Means clustering on the normal vectors within \mathcal{S}_{flat} to identify the global geometric trend. The centroid of the largest cluster is defined as the Dominant Normal \mathbf{n}_{dom} , representing the principal horizontal plane (i.e., rooftops and ground). The geometric consistency C_{geo} for each spatial location (i, j) is then computed as the cosine similarity to this dominant centroid:

$$C_{geo}^{(i,j)} = \mathbf{n}^{(i,j)} \cdot \mathbf{n}_{dom}. \quad (6)$$

This formulation ensures that rooftop regions (belonging to the dominant cluster) yield high consistency scores ($C_{geo} \rightarrow 1$), whereas vertical facades deviate significantly ($C_{geo} \ll 1$).

4) *Adaptive Gating with Neutral Edge Rectification*: Geometry varies significantly across urban scenes. We introduce a learnable gating mechanism to map the consistency score to an attention mask. A differentiable sigmoid function with learnable scale α and bias β dynamically calibrates the filtering intensity:

$$\mathcal{M}_{raw} = \sigma(\alpha \cdot C_{geo} + \beta). \quad (7)$$

Crucially, to prevent erroneous suppression or enhancement in ambiguous regions, we apply a Neutral Edge Rectification

strategy. For pixels identified as edges (\mathcal{E}), the attention weight is explicitly reset to a neutral value (0.5), ensuring non-destructive modulation. The final geometric mask \mathcal{M}_{geo} is derived as:

$$\mathcal{M}_{geo}^{(i,j)} = \begin{cases} 0.5, & \text{if } (i, j) \in \mathcal{E} \\ \mathcal{M}_{raw}^{(i,j)}, & \text{otherwise} \end{cases}. \quad (8)$$

5) *Residual Geometric Modulation*: Finally, we inject this geometric prior into the semantic stream via a residual modulation:

$$\tilde{F}_u = F_u \odot (1 + \mathcal{M}_{geo}). \quad (9)$$

By strictly amplifying valid structural features while neutralizing edges and suppressing facades, MGSF significantly enhances the signal-to-noise ratio of co-visible structures.

D. Geometric-Appearance Contrastive Distillation (GACD) Loss

While MGSF enhances features in the forward pass, the backbone network itself may still implicitly overfit to prominent vertical textures (e.g., illuminated windows). Regressing exact depth values to correct this is ill-posed due to scale ambiguity. Instead, we propose GACD, a ranking-based loss that reformulates geometric alignment as a relative ordering problem. The intuition is simple yet powerful: The average feature activation on positive anchors must be strictly stronger than on hard negatives.

1) *Geometric Partitioning*: Using the mask \mathcal{M}_{geo} generated by MGSF, we dynamically partition the feature map spatial locations $\Omega = \{(i, j)\}$ into a Co-visible Set \mathcal{P} and an "Occlusion Set" \mathcal{N} based on confidence quantiles:

$$\mathcal{P} = \{(i, j) \mid \mathcal{M}_{geo}^{(i,j)} > \tau_{high}\}, \quad (10)$$

$$\mathcal{N} = \{(i, j) \mid \mathcal{M}_{geo}^{(i,j)} < \tau_{low}\}, \quad (11)$$

where τ_{high} and τ_{low} are thresholds determining the most confident geometric regions.

2) *Activation Aggregation*: We define the activation map A_{sem} as the channel-wise magnitude of the enhanced features \tilde{F}_u :

$$A_{sem}^{(i,j)} = \frac{1}{C} \sum_{k=1}^C \|\tilde{F}_u^{(k,i,j)}\|_2. \quad (12)$$

We then compute the mean activation intensity for the partitioned sets:

$$v_{rooftop} = \frac{1}{|\mathcal{P}|} \sum_{(i,j) \in \mathcal{P}} A_{sem}^{(i,j)}, \quad v_{wall} = \frac{1}{|\mathcal{N}|} \sum_{(i,j) \in \mathcal{N}} A_{sem}^{(i,j)}. \quad (13)$$

3) *Contrastive Ranking Objective*: The GACD loss enforces a margin between these two aggregates. It penalizes the network whenever the semantic attention on vertical facades approaches or exceeds the attention on rooftops:

$$\mathcal{L}_{GACD} = \max(0, \xi + v_{wall} - v_{rooftop}), \quad (14)$$

where ξ is a predefined margin. Unlike depth regression losses (e.g., MSE) that punish numerical inaccuracies, \mathcal{L}_{GACD} acts as a semantic rectifier. It allows the network

to ignore the exact depth value as long as it correctly learns to suppress vertical features and highlight horizontal ones. This effectively distills the geometric prior into the semantic encoder, making the representation inherently robust to view changes.

E. Optimization Objective

The overall training objective combines the primary retrieval loss with our geometric constraint:

$$\mathcal{L}_{total} = \mathcal{L}_{triplet} + \lambda_{geo} \mathcal{L}_{GACD}, \quad (15)$$

where $\mathcal{L}_{triplet}$ is the weighted soft-margin triplet loss ensuring discrimination between matching and non-matching places, and λ_{geo} balances the geometric regularization.

IV. EXPERIMENTS

A. Datasets and Evaluation Metrics

To rigorously evaluate the effectiveness of the proposed framework, we conducted experiments on two standard benchmarks: University-1652 [38] and SUES-200 [39].

University-1652 is a large-scale multi-view dataset containing 1,652 buildings from 72 universities. It includes 50,218 drone-view images for training and 37,855 for testing, paired with corresponding satellite orthophotos. This dataset is particularly challenging due to the inclusion of drone images captured at varying distances and angles.

SUES-200 focuses on multi-altitude scenarios, covering 200 disparate locations. It provides drone images captured at four distinct altitudes (150m, 200m, 250m, and 300m). This stratified height design allows for a fine-grained assessment of the model’s robustness against scale variations.

Following standard protocols, we employ Recall at K (R@K) and Average Precision (AP) as the primary metrics. R@K measures the percentage of query images for which the ground truth is retrieved within the top-K predictions, while AP evaluates the precision of the retrieval ranking.

B. Implementation Details

We implemented (MGS)² using the PyTorch framework on a single NVIDIA GeForce A800 GPU. During the training phase, the input images for both satellite and drone views were resized to 224×224 . For inference, we adopted a higher resolution of 336×336 to capture finer-grained geometric details. We utilized a pre-trained DINOv2 as the backbone to extract initial semantic features. We used AdamW with weight decay $9.5e-9$. A linear learning rate schedule was applied. The batch size was 128. We employed parameter-wise learning rates: $6e-6$ for the RGB backbone, $5e-5$ for depth-related modules (depth encoder + MGSF + MGSA), and $1e-4$ for the aggregator. The hyper-parameters for GACD loss, λ_{geo} and margin ξ , were empirically set to 1.0 and 0.5, respectively. During inference, we utilized the cosine similarity of the final fused embeddings for retrieval ranking.

TABLE I
PERFORMANCE COMPARISON ON THE UNIVERSITY-1652 DATASET. THE
BEST RESULTS ARE IN **BOLD**.

| Method | Publication | Drone → Satellite | | Satellite → Drone | |
|---------------------------------|-------------|-------------------|--------------|-------------------|--------------|
| | | R@1 | AP | R@1 | AP |
| TransFG [40] | TGRS’24 | 84.01 | 86.31 | 90.16 | 84.61 |
| MJRLIFS [7] | TGRS’24 | 86.06 | 88.08 | 91.44 | 85.73 |
| GeoFormer [21] | JSTARS’24 | 89.08 | 90.83 | 92.30 | 88.54 |
| SeGCN [23] | JSTARS’24 | 89.18 | 90.89 | 94.29 | 89.65 |
| MCCG [41] | TCSVT’23 | 89.64 | 91.32 | 94.30 | 89.39 |
| SDPL [42] | TCSVT’24 | 90.16 | 91.64 | 93.58 | 89.45 |
| CCR [43] | TCSVT’24 | 92.54 | 93.78 | 95.15 | 91.80 |
| Sample4Geo [17] | ICCV’23 | 92.65 | 93.81 | 96.43 | 93.79 |
| SRLN [22] | TGRS’24 | 92.70 | 93.77 | 95.14 | 91.97 |
| MEAN [28] | TGRS’25 | 93.55 | 94.53 | 96.01 | 92.08 |
| SCOF [44] | TGRS’25 | 93.68 | 94.68 | 96.29 | 92.68 |
| CAMP [11] | TGRS’24 | 94.46 | 95.38 | 96.15 | 92.72 |
| DAC [45] | TCSVT’24 | 94.67 | 95.50 | 96.43 | 93.79 |
| QDFL [29] | TGRS’25 | 95.00 | 95.83 | 97.15 | 94.57 |
| CDM-Net [31] | TGRS’25 | 95.13 | 96.04 | 96.43 | 93.79 |
| (MGS)² (Ours) | — | 97.50 | 97.97 | 98.57 | 97.27 |

C. Comparison with State-of-the-Art Methods

1) *Performance on University-1652*: We compared (MGS)² against recent state-of-the-art (SOTA) methods, including geometric-aware approaches like GeoFormer and semantic-enhanced methods like CAMP and QDFL. The quantitative results are summarized in Table I.

It is evident that (MGS)² achieves superior performance across all metrics. Specifically, in the Drone → Satellite task, our method achieves a Recall@1 of 97.50% and an AP of 97.97%. This represents a significant improvement over the runner-up CDM-Net [31] (+2.37% in R@1) and QDFL (+2.50% in R@1). Unlike methods that treat the image as a 2D plane, our framework explicitly models the 3D macro-structure. The substantial gain in AP indicates that our MGSF module effectively purifies the feature space, ensuring that hard-negative facade features do not confuse the retrieval ranking.

2) *Robustness to Scale Variations on SUES-200*: We also evaluated our method on SUES-200 across different flight altitudes. As shown in Table II, (MGS)² exhibits remarkable stability. While most existing methods (e.g., MJRLIFS, SeGCN) suffer from performance degradation at lower altitudes (150m) due to the impact of more vertical facades, (MGS)² maintains a high R@1 of 97.02% at 150m on the Drone → Satellite task. As the altitude increases to 300m, our performance reaches near-saturation (99.78% R@1). The reason for maintaining extremely high recall at high altitudes is that our deep guidance scale fusion provides a more physically grounded solution to scale ambiguity. Compared to MEAN [28], which employs multi-level embeddings, our approach still outperforms it at 300m altitude. Notably, on the Satellite → Drone task, apart from the challenging 150m altitude, all other altitudes have achieved 100% R@1. This indicates that the localization task in this scenario has been resolved. These results confirm that (MGS)² successfully

TABLE II
PERFORMANCE COMPARISON BETWEEN DIFFERENT METHODS ON DRONE-TO-SATELLITE AND SATELLITE-TO-DRONE RETRIEVAL TASKS

| Drone→Satellite | | | | | | | | | |
|---------------------------------|-------------|--------------|--------------|---------------|--------------|---------------|--------------|---------------|--------------|
| Method | Publication | 150m | | 200m | | 250m | | 300m | |
| | | R@1 | AP | R@1 | AP | R@1 | AP | R@1 | AP |
| SUES-200 [39] | TCSVT'23 | 59.32 | 64.93 | 62.30 | 67.24 | 71.35 | 75.49 | 77.17 | 67.80 |
| MJRLIFS [46] | TGRS'24 | 77.57 | 81.30 | 89.50 | 91.40 | 92.58 | 94.21 | 97.40 | 97.92 |
| SeGCN [23] | JSTARS'24 | 90.80 | 92.32 | 91.93 | 93.41 | 92.53 | 93.90 | 93.33 | 94.61 |
| MCCG [41] | TCSVT'23 | 82.22 | 85.47 | 89.38 | 91.41 | 93.82 | 95.04 | 95.07 | 96.20 |
| SDPL [42] | TCSVT'24 | 82.95 | 85.82 | 92.73 | 94.07 | 96.05 | 96.69 | 97.83 | 98.05 |
| CCR [43] | TCSVT'24 | 87.08 | 89.55 | 93.57 | 94.90 | 95.42 | 96.28 | 96.82 | 97.39 |
| Sample4Geo [17] | ICCV'23 | 92.60 | 96.38 | 97.38 | 97.81 | 98.28 | 98.64 | 99.18 | 99.36 |
| SRLN [22] | TGRS'24 | 89.90 | 91.90 | 94.32 | 95.65 | 95.92 | 96.79 | 96.37 | 97.21 |
| SCOF [44] | TGRS'25 | 90.75 | 92.32 | 94.25 | 95.35 | 96.88 | 97.42 | 97.85 | 98.10 |
| QDFL [29] | TGRS'25 | 93.97 | 95.42 | 98.25 | 98.67 | 99.30 | 99.48 | 99.31 | 99.48 |
| CDM-Net [31] | TGRS'25 | 93.78 | 95.16 | 97.62 | 98.16 | 98.28 | 98.69 | 99.20 | 99.31 |
| CAMP [11] | TGRS'24 | 95.40 | 96.38 | 97.63 | 98.16 | 98.05 | 98.45 | 99.33 | 99.46 |
| MEAN [28] | TGRS'25 | 95.50 | 96.46 | 98.38 | 98.72 | 98.95 | 99.17 | 99.52 | 99.63 |
| DAC [45] | TCSVT'24 | 96.80 | 97.54 | 97.48 | 97.97 | 98.20 | 98.62 | 97.58 | 98.14 |
| (MGS)² (Ours) | — | 97.02 | 97.86 | 99.52 | 99.61 | 99.67 | 99.75 | 99.78 | 99.83 |
| Satellite→Drone | | | | | | | | | |
| Method | Publication | 150m | | 200m | | 250m | | 300m | |
| | | R@1 | AP | R@1 | AP | R@1 | AP | R@1 | AP |
| SUES-200 | TCSVT'23 | 82.50 | 58.95 | 85.00 | 62.56 | 88.75 | 69.96 | 96.25 | 84.16 |
| MJRLIFS | TGRS'24 | 93.75 | 79.49 | 97.50 | 90.52 | 97.50 | 96.03 | 100.00 | 97.66 |
| SeGCN | JSTARS'24 | 93.75 | 92.45 | 95.00 | 93.65 | 96.25 | 94.39 | 97.50 | 94.55 |
| MCCG | TCSVT'23 | 93.75 | 89.72 | 93.75 | 92.21 | 96.25 | 96.14 | 98.75 | 96.64 |
| SDPL | TCSVT'24 | 93.75 | 83.75 | 96.25 | 92.42 | 97.50 | 95.65 | 96.25 | 96.17 |
| CCR | TCSVT'24 | 92.50 | 88.54 | 97.50 | 95.22 | 97.50 | 97.10 | 97.50 | 97.49 |
| Sample4Geo | ICCV'23 | 97.50 | 93.63 | 98.75 | 96.70 | 98.75 | 98.28 | 98.75 | 98.05 |
| SRLN | TGRS'24 | 93.75 | 93.01 | 97.50 | 95.08 | 97.50 | 96.52 | 97.50 | 96.71 |
| SCOF | TGRS'25 | 95.00 | 89.72 | 97.50 | 93.13 | 98.75 | 96.33 | 97.50 | 96.62 |
| CDM-Net | TGRS'25 | 95.25 | 92.24 | 98.50 | 96.40 | 99.00 | 97.60 | 99.00 | 98.01 |
| CAMP | TGRS'24 | 96.25 | 93.69 | 97.50 | 96.76 | 98.75 | 98.10 | 100.00 | 98.85 |
| DAC | TCSVT'24 | 97.50 | 94.06 | 98.75 | 96.66 | 98.75 | 98.09 | 98.75 | 97.87 |
| MEAN | TGRS'25 | 97.50 | 94.75 | 100.00 | 97.09 | 100.00 | 98.28 | 100.00 | 99.21 |
| QDFL | TGRS'25 | 98.75 | 95.10 | 98.75 | 97.92 | 100.00 | 99.07 | 100.00 | 99.07 |
| (MGS)² (Ours) | — | 98.95 | 95.31 | 100.00 | 98.38 | 100.00 | 99.17 | 100.00 | 99.18 |

TABLE III
GENERALIZATION FROM UNIVERSITY-1652 TO DENSEUAV

| Method | UAV→Satellite | | Satellite→UAV | |
|---------------------------------|---------------|--------------|---------------|--------------|
| | R@1 | AP | R@1 | AP |
| Sample4Geo | 22.00 | 14.58 | 19.10 | 17.46 |
| CAMP | 23.48 | 15.75 | 20.97 | 20.29 |
| SURFNet (Zero shot) | 24.28 | 16.13 | 21.04 | 20.37 |
| SURFNet (Fine-tune) | 71.06 | 65.99 | 87.43 | 51.29 |
| (MGS)² (Ours) | 81.70 | 84.49 | 91.25 | 78.99 |

achieved cross-view geo-location through two carefully designed components.

3) *Cross-Dataset Generalization*: A critical bottleneck for learning-based CVGL is overfitting to the source domain's

specific architecture style. To test generalization, we trained our model on University-1652 and directly evaluated it on the DenseUAV dataset (Table III).

In the zero-shot/transfer setting, most methods collapse. SURFNet believes DenseUAV possesses stronger photometric/stylistic transfer capabilities and denser urban coverage, while other methods face challenges in generalizing on this dataset. For instance, CAMP yields only 23.48% R@1. In contrast, our method achieves a Recall@1 of 81.70%. This dramatic margin suggests that (MGS)² learns geometric properties rather than dataset-specific texture patterns. By filtering out non-transferable vertical facades, the model focuses on the structural "fingerprint" of buildings, which is invariant across cities.

TABLE IV
COMPONENT-WISE ABLATION ANALYSIS ON UNIVERSITY-1652

| Model | Baseline | MGSA | MGSF | GSCD | R@1 | AP |
|-----------|----------|------|------|------|--------------|--------------|
| I (Base) | ✓ | | | | 94.xx | 95.xx |
| II | ✓ | ✓ | | | 95.xx | 96.xx |
| III | ✓ | ✓ | ✓ | | 96.xx | 97.xx |
| IV (Full) | ✓ | ✓ | ✓ | ✓ | 97.50 | 97.97 |

D. Ablation Studies

To dissect the contribution of each component in $(MGS)^2$, we conducted comprehensive ablation studies on the University-1652 dataset.

1) Effectiveness of Macro-Geometric Structure Filtering (MGSF): The MGSF module is the core of our proposal. As illustrated in the ablation results, removing MGSF leads to a noticeable drop in performance (e.g., R@1 decreases from 97.5% to ~95%). Without MGSF, the network naively attends to prominent vertical features like windows or billboards. These features are highly salient in drone views but non-existent in satellite views, acting as distractors.

2) Impact of Micro-Geometric Scale Adaptation (MGSA): The MGSA module is crucial for handling altitude changes. We observed that replacing MGSA with a simple multi-scale concatenation results in slower convergence and lower accuracy, particularly on the SUES-200 dataset. MGSA utilizes depth priors to dynamically re-weight features, allowing the network to focus on the appropriate spatial frequency corresponding to the physical distance, thereby resolving micro-scale ambiguity.

E. Qualitative Analysis and Visualization

To provide intuitive insights into how $(MGS)^2$ bridges the domain gap, we present visualizations of feature responses and retrieval results.

Fig. 3 visualizes the feature activation maps before and after applying MGSF. By comparison, it demonstrates the calculation of the final enhanced feature heatmap (d) using both the computed zenith normal map (b) and the baseline feature heatmap (c). The zenith normality map (b) clearly demonstrates that MGSF successfully predicts horizontal planes (white area) and vertical planes (black area). Using this as a mask, it forces the feature map to focus more on horizontal plane features rather than vertical plane features. This is also well represented on the feature map: horizontal planes (roofs, road surfaces, etc.) within the white box are effectively enhanced, while vertical planes within the black box are suppressed. This confirms that MGSF functions not merely as an attention mechanism, but as a physical filter that aligns the drone view with the orthographic satellite reference.

1) Visualization of Geometric Filtering: We further compared the top 5 retrieval results between the baseline and $(MGS)^2$ and selected representative examples as shown in Figure 4. As demonstrated in the second and fourth rows, the baseline (DINOv2 + SALAD) frequently retrieves candidates with similar facade textures but differing structural layouts, leading to false positives. For instance, in the UAV \rightarrow Satellite

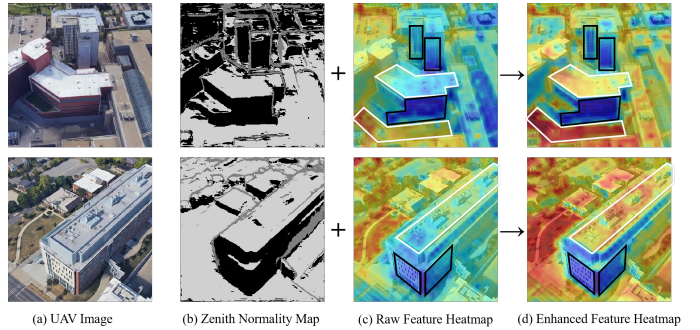


Fig. 3. Visualization of the Macro-Geometric Structure Filtering (MGSF) Mechanism. We visualize the feature response maps before and after applying MGSF. (a) Original Features: The backbone naively activates on high-frequency vertical textures. (b) Enhanced Features: MGSF redistributes attention based on geometric priors. Note that black boxes indicate the effective suppression of view-dependent vertical facades, while white boxes highlight the adaptive enhancement of view-invariant Horizontal planes.

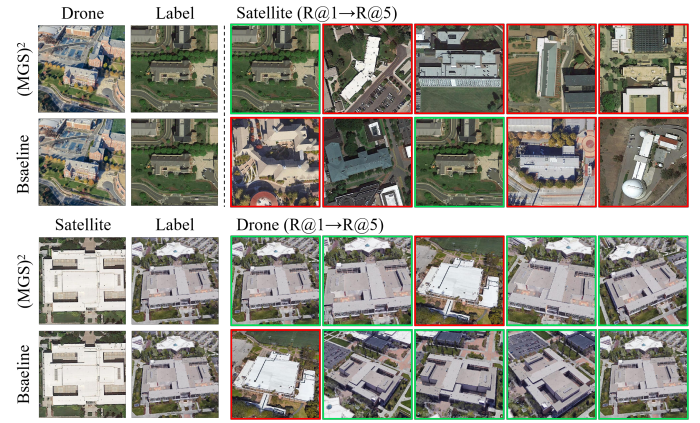


Fig. 4. Qualitative image retrieval results for the University-1652 dataset. (Top) Top 5 retrieval results for target localization in drone view. (Bottom) Top 5 retrieval results for drone navigation. The first and third rows show retrieval results for $(MGS)^2$; the second and fourth rows show retrieval results for the baseline (DINOv2 + SALAD). Green boxes indicate correctly-matched images; red boxes indicate incorrectly-matched images.

task, the baseline (row 2) tends to recall results containing red features during retrieval because the query facade texture exhibits red features. In contrast, $(MGS)^2$ (row 1) correctly retrieves the target location while ignoring the red texture. In the Satellite \rightarrow UAV task, a challenging case involves a roof with large white 2D features. $(MGS)^2$ actively focuses on the roof structure while suppressing excessive RGB influence, yielding correct R@1. This is particularly evident in densely packed high-rise scenarios, where our method's ability to distinguish inclination proves crucial for accurate localization.

V. CONCLUSION

In this paper, we presented $(MGS)^2$, a geometry-grounded framework that bridges the UAV-satellite domain gap by shifting from 2D appearance matching to 3D structural alignment. By synergizing the Macro-Geometric Structure Filtering (MGSF) to suppress vertical artifacts and the Micro-Geometric Scale Adaptation (MGSA) to rectify scale discrepancies, our method effectively extracts view-invariant

geometric features. Extensive experiments demonstrate that (MGS)² achieves state-of-the-art performance on University-1652 and SUES-200 benchmarks. Future work will focus on distilling the geometric awareness into a lightweight backbone for real-time edge deployment and improving robustness against extreme illumination variations.

REFERENCES

- [1] Yuekuan Zhou. Unmanned aerial vehicles based low-altitude economy with lifecycle techno-economic-environmental analysis for sustainable and smart cities. *Journal of Cleaner Production*, 499:145050, 2025.
- [2] Tazeem Ahmad, Alicia Esquivel Morel, Nuo Cheng, Kannappan Palaniappan, Prasad Calyam, Kun Sun, and Jianli Pan. Future uav/drone systems for intelligent active surveillance and monitoring. *ACM Computing Surveys*, 58(2):35:1–35:37, 2026.
- [3] Yujiao Shi, Xin Yu, Liu Liu, Dylan Campbell, Piotr Koniusz, and Hongdong Li. Accurate 3-dof camera geo-localization via ground-to-satellite image matching. *IEEE transactions on pattern analysis and machine intelligence*, 45(3):2682–2697, 2022.
- [4] Xiuw Zhang, Lei Wang, and Yan Su. Visual place recognition: A survey from deep learning perspective. *Pattern Recognition*, 113:107760, 2021.
- [5] Guopeng Li, Ming Qian, and Gui-Song Xia. Unleashing unlabeled data: A paradigm for cross-view geo-localization. In *Proceedings of the IEEE/CVF Conference on Computer Vision and Pattern Recognition (CVPR)*, pages 16719–16729, June 2024.
- [6] Zhedong Zheng, Yunchao Wei, and Yi Yang. University-1652: A multi-view multi-source benchmark for drone-based geo-localization. In *Proceedings of the 28th ACM international conference on Multimedia*, pages 1395–1403, 2020.
- [7] Tingyu Wang, Zhenzheng Cheng, Chenggang Yan, Jiyong Zhang, Yaoqi Sun, Bolun Zheng, and Yi Yang. Each part matters: Local patterns facilitate cross-view geo-localization. *IEEE Transactions on Circuits and Systems for Video Technology*, 32(2):867–879, 2021.
- [8] Yujiao Shi, Liu Liu, Xin Yu, and Hongdong Li. Spatial-aware feature aggregation for cross-view image based geo-localization. *Advances in Neural Information Processing Systems*, 32, 2019.
- [9] Sijie Zhu, Mubarak Shah, and Chen Chen. Transgeo: Transformer is all you need for cross-view image geo-localization. In *Proceedings of the IEEE/CVF Conference on Computer Vision and Pattern Recognition*, pages 1162–1171, 2022.
- [10] Hongji Yang, Xiufan Lu, and Yingying Zhu. Cross-view geo-localization with layer-to-layer transformer. *Advances in Neural Information Processing Systems*, 34:29009–29020, 2021.
- [11] Qiong Wu, Yi Wan, Zhi Zheng, Yongjun Zhang, Guangshuai Wang, and Zhenyang Zhao. Camp: A cross-view geo-localization method using contrastive attributes mining and position-aware partitioning. *IEEE Transactions on Geoscience and Remote Sensing*, 2024.
- [12] Cheng Fang, Jingchun Gao, Ping Han, Chaoyu Zhao, and Bing Gao. Scof: Supervised contrastive orthogonal fusion for robust cross-view geolocalization. *IEEE Transactions on Geoscience and Remote Sensing*, 63:1–15, 2025.
- [13] Kun Liu and Wensheng Zhang. Surfnet: A surface-aware uav–satellite geolocation framework via feature aggregation and dual positional encoding. *IEEE Transactions on Geoscience and Remote Sensing*, 64:1–15, 2026.
- [14] Krishna Regmi and Mubarak Shah. Bridging the domain gap for ground-to-aerial image matching. In *Proceedings of the IEEE/CVF International Conference on Computer Vision*, pages 470–479, 2019.
- [15] Sixing Hu, Mengdan Feng, Rang MH Nguyen, and Gim Hee Lee. Cvm-net: Cross-view matching network for image-based ground-to-aerial geo-localization. In *Proceedings of the IEEE Conference on Computer Vision and Pattern Recognition*, pages 7258–7267, 2018.
- [16] Jinliang Lin, Zhenzheng Zheng, Zhun Zhong, Zhiming Luo, Shaozi Li, Yi Yang, and Nicu Sebe. Joint representation learning and keypoint detection for cross-view geo-localization. *IEEE Transactions on Image Processing*, 31:3780–3792, 2022.
- [17] Fabian Deuser, Konrad Habel, and Norbert Oswald. Sample4geo: Hard negative sampling for cross-view geo-localisation. In *Proceedings of the IEEE/CVF International Conference on Computer Vision*, pages 16847–16856, 2023.
- [18] Mathilde Caron, Hugo Touvron, Ishan Misra, Hervé Jégou, Julien Mairal, Piotr Bojanowski, and Armand Joulin. Emerging properties in self-supervised vision transformers. In *Proceedings of the IEEE/CVF international conference on computer vision*, pages 9650–9660, 2021.
- [19] Maxime Oquab, Timothée Darcret, Théo Moutakanni, Huy Vo, Marc Szafraniec, Vasil Khalidov, Pierre Fernandez, Daniel Haziza, Francisco Massa, Alaeldin El-Nouby, et al. Dinov2: Learning robust visual features without supervision. *arXiv preprint arXiv:2304.07193*, 2023.
- [20] Nikhil Keetha, Avneesh Mishra, Jay Karhade, Krishna Murthy Jatavallabula, Sebastian Scherer, Madhava Krishna, and Sourav Garg. Anyloc: Towards universal visual place recognition. *IEEE Robotics and Automation Letters*, 9(2):1286–1293, 2023.
- [21] Qingge Li, Xiaogang Yang, Jiwei Fan, Ruitao Lu, Bin Tang, Siyu Wang, and Shuang Su. Geoformer: An effective transformer-based siamese network for uav geolocalization. *IEEE Journal of Selected Topics in Applied Earth Observations and Remote Sensing*, 17:9470–9491, 2024.
- [22] Hongxiang Lv, Hai Zhu, Runzhe Zhu, Fei Wu, Chunyuan Wang, Meiyu Cai, and Kaiyu Zhang. Direction-guided multiscale feature fusion network for geo-localization. *IEEE Transactions on Geoscience and Remote Sensing*, 62:1–13, 2024.
- [23] Xiangzeng Liu, Ziyao Wang, Yue Wu, and Qiguang Miao. Segcn: A semantic-aware graph convolutional network for uav geo-localization. *IEEE Journal of Selected Topics in Applied Earth Observations and Remote Sensing*, 17:6055–6066, 2024.
- [24] Yuan Gao, Haibo Liu, and Xiaohui Wei. Semantic concept perception network with interactive prompting for cross-view image geo-localization. *IEEE Transactions on Circuits and Systems for Video Technology*, 2025.
- [25] Ziqian Mo, Yuxi Sun, Meng Xu, and Sen Jia. Sign: Saliency-aware integrated global-local network for cross-view geo-localization. In *IGARSS 2025-2025 IEEE International Geoscience and Remote Sensing Symposium*, pages 6296–6300. IEEE, 2025.
- [26] Tingyu Wang, Zhenzheng Cheng, Yaoqi Sun, Chenggang Yan, Yi Yang, and Tat-Seng Chua. Multiple-environment self-adaptive network for aerial-view geo-localization. *Pattern Recognition*, 152:110363, 2024.
- [27] Jian Sun, Kangdao Liu, Chi Zhang, Chuangquan Chen, Junge Shen, C. L. Philip Chen, and Chi-Man Vong. Mobilegeo: Exploring hierarchical knowledge distillation for resource-efficient cross-view drone geo-localization, 2026.
- [28] Zhongwei Chen, Zhao-Xu Yang, and Hai-Jun Rong. Multi-level embedding and alignment network with consistency and invariance learning for cross-view geo-localization. *IEEE Transactions on Geoscience and Remote Sensing*, 2025.
- [29] Shuyu Hu, Zelin Shi, Tong Jin, and Yunpeng Liu. Query-driven feature learning for cross-view geo-localization. *IEEE Transactions on Geoscience and Remote Sensing*, 2025.
- [30] Sijie Zhu, Linjie Yang, Chen Chen, Mubarak Shah, Xiaohui Shen, and Heng Wang. R2former: Unified retrieval and reranking transformer for place recognition. In *Proceedings of the IEEE/CVF Conference on Computer Vision and Pattern Recognition*, pages 19370–19380, 2023.
- [31] Xin Zhou, Xuerong Yang, and Yanchun Zhang. Cdm-net: A framework for cross-view geo-localization with multimodal data. *IEEE Transactions on Geoscience and Remote Sensing*, 2025.
- [32] Sijie Wang, Rui She, Qiyu Kang, Siqi Li, Disheng Li, Tianyu Geng, Shangshu Yu, and Wee Peng Tay. Multi-modal aerial-ground cross-view place recognition with neural odes. In *Proceedings of the Computer Vision and Pattern Recognition Conference*, pages 11717–11728, 2025.
- [33] Zijie Zhou, Jingyi Xu, Guangming Xiong, and Junyi Ma. Lcpr: A multi-scale attention-based lidar-camera fusion network for place recognition. *IEEE Robotics and Automation Letters*, 9(2):1342–1349, 2023.
- [34] Alex Junho Lee, Seungwon Song, Hyungtae Lim, Woojoo Lee, and Hyun Myung. (lc)²: Lidar-camera loop constraints for cross-modal place recognition. *IEEE Robotics and Automation Letters*, 8(6):3589–3596, 2023.
- [35] Abhilash Durgam, Sidike Paheding, Vikas Dhiman, and Vijay Devabhaktuni. Cross-view geo-localization: a survey. *IEEE Access*, 2024.
- [36] Yujiao Shi, Xin Yu, Liu Liu, Tong Zhang, and Hongdong Li. Optimal feature transport for cross-view image geo-localization. In *Proceedings of the AAAI Conference on Artificial Intelligence*, volume 34, pages 11990–11997, 2020.
- [37] Haotong Lin, Sili Chen, Junhao Liew, Donny Y Chen, Zhenyu Li, Guang Shi, Jiashi Feng, and Bingyi Kang. Depth anything 3: Recover-

ing the visual space from any views. *arXiv preprint arXiv:2511.10647*, 2025.

[38] Zhedong Zheng, Yunchao Wei, and Yi Yang. University-1652: A multi-view multi-source benchmark for drone-based geo-localization. In *Proceedings of the 28th ACM International Conference on Multimedia*, pages 1395–1403, 2020.

[39] Runzhe Zhu, Ling Yin, Mingze Yang, Fei Wu, Yuncheng Yang, and Wenbo Hu. Sues-200: A multi-height multi-scene cross-view image benchmark across drone and satellite. *IEEE Transactions on Circuits and Systems for Video Technology*, 33(12):7667–7680, 2023.

[40] Hu Zhao, Keyan Ren, Tianyi Yue, Chun Zhang, and Shuai Yuan. Transfg: A cross-view geo-localization of satellite and uavs imagery pipeline using transformer-based feature aggregation and gradient guidance. *IEEE Transactions on Geoscience and Remote Sensing*, 62:1–12, 2024.

[41] Tianrui Shen, Yingmei Wei, Lai Kang, Shanshan Wan, and Yee-Hong Yang. Mccg: A convnext-based multiple-classifier method for cross-view geo-localization. *IEEE Transactions on Circuits and Systems for Video Technology*, 34(3):1456–1468, 2023.

[42] Quan Chen, Tingyu Wang, Zihao Yang, Haoran Li, Rongfeng Lu, Yaoqi Sun, Bolun Zheng, and Chenggang Yan. Sdpl: Shifting-dense partition learning for uav-view geo-localization. *IEEE Transactions on Circuits and Systems for Video Technology*, 34(11):11810–11824, 2024.

[43] Haolin Du, Jingfei He, and Yuanqing Zhao. Ccr: A counterfactual causal reasoning-based method for cross-view geo-localization. *IEEE Transactions on Circuits and Systems for Video Technology*, 2024.

[44] Cheng Fang, Jingchun Gao, Ping Han, Chaoyu Zhao, and Bing Gao. Scof: Supervised contrastive orthogonal fusion for robust cross-view geolocalization. *IEEE Transactions on Geoscience and Remote Sensing*, 63:1–15, 2025.

[45] Panwang Xia, Yi Wan, Zhi Zheng, Yongjun Zhang, and Jiwei Deng. Enhancing cross-view geo-localization with domain alignment and scene consistency. *IEEE Transactions on Circuits and Systems for Video Technology*, 2024.

[46] Fawei Ge, Yunzhou Zhang, Yixiu Liu, Guiyuan Wang, Sonya Coleman, Dermot Kerr, and Li Wang. Multibranch joint representation learning based on information fusion strategy for cross-view geo-localization. *IEEE Transactions on Geoscience and Remote Sensing*, 62:1–16, 2024.